NASA TECHNICAL MEMORANDUM 89091

STRAIN-ENERGY RELEASE RATE ANALYSIS OF A LAMINATE WITH A POSTBUCKLED DELAMINATION

JOHN D. WHITCOMB AND K. N. SHIVAKUMAR

FEBRUARY 1987

NASA

National Aeronautics and Space Administration

Langley Research Center
Hampton, Virginia 23665

INTRODUCTION

Localized buckling of a delaminated group of plies creates high interlaminar stresses around the boundary of the delamination. This often causes rapid, extensive delamination growth. A measure of the intensity of the interlaminar stresses at the delamination boundary is needed to predict delamination growth. Since the stresses at the delamination boundary are singular (at least mathematically), calculated stresses there have little meaning. Strain-energy release rates are finite parameters which characterize the intensity of the stresses near the singularity. Hence, many of the current efforts to predict instability-related delamination growth are based on strain-energy release rates.

The problem of instability-related delamination growth has been studied both experimentally [eg. refs. 1-4] and analytically [eg. refs. 3-7]. The predominant configurations analyzed have been either a laminate with a through-width or embedded delamination (see fig. 1). In this paper the embedded delamination will be considered.

For the through-width delamination, both 2-D finite element [ref. 5] and Rayleigh-Ritz beam [ref. 7] solutions have been obtained. To date, strain-energy release rate analysis of the embedded delamination has been limited to using plate analysis to calculate the average value of the total strain-energy release rate G along a delamination front. The total strain-energy release rate is simply the sum of the mode I, mode II and mode III components. Ideally, one would like to obtain the magnitudes of the individual components. But such is beyond the scope of plate analysis; expensive three-dimensional analysis would be required. The current study also used plate analysis, so only total G was calculated. However, in contrast to earlier work, the present study calculated distributions of G along the delamination front. The distribution of G was calculated using a new virtual crack closure technique which is suitable for use with plate analysis.

The objectives of this paper are to present the derivation of the new virtual crack closure technique, evaluate the accuracy of the technique, and finally to present the results of a limited parametric study of laminates with a postbuckled delamination. Although the new virtual crack closure technique is general, only homogeneous, isotropic laminates were analyzed in this paper. This was to eliminate the variation of flexural stiffness with orientation, which occurs even for quasi-isotropic laminates. This made it easier to identify the effect of geometrical parameters on G.

In the following sections the new virtual crack closure technique will be derived first. Then the specimen configurations will be described. Next, the stress analyses will be discussed. Finally, the virtual crack closure technique will be evaluated and then used to calculate the distribution of G along the delamination front of several laminates with a postbuckled delamination.

NOMENCLATURE

[A], [B], [D]	submatrices in laminate theory constitutive relations
a,b	length of delamination in x- and y-directions, respectively, mm
D_{11}	flexural stiffness coefficient = $Eh^3/(12(1-\nu^2))$, Nm
e_o	strain in x-direction in base laminate
e_{CR}	e_o for buckling of sublaminate
E	Young's modulus, N/m^2
G	total strain-energy release rate, J/m^2
G_{av}	average strain-energy release rate, J/m^2
G_M	strain-energy release rate due to moment, J/m^2
G_N	strain-energy release rate due to in-plane stress resultants, J/m^2
k	curvature
M, M_x, M_y, M_{xy}	moment resultants, Nm/m
N_x, N_y	in-plane stress resultants, N/m
P	point load, N
u,v,w	displacements in x, y, and z directions, m
w_o	transverse displacement at the center of the square laminated plate, m
x,y,z	rectangular Cartesian coordinates
ε	strain
ν	Poisson's ratio

ANALYSIS

The following subsections describe the new virtual crack closure technique (VCCT), the configurations analyzed, and the stress analyses used in conjunction with the VCCT.

New Virtual Crack Closure Technique

The basic tenet of any crack closure technique is that strain-energy release rate is equal to the work per unit area required to close a crack over a small distance. For a 3-D configuration, such as that in figure 2, the strain-energy release rate is calculated using an equation of the following form [ref. 9].

$$G = \lim_{\Delta a \to o} \frac{1}{2\Delta a} \int_{o}^{\Delta a} \left[\sigma_z(x - \Delta a)w(x) + \sigma_{xz}(x - \Delta a)u(x) + \sigma_{yz}(x - \Delta a)v(x)\right] dx \tag{1}$$

where Δa is the crack closure length, u, v, and w are the displacements in the x, y, and z directions, and σ_z, σ_{xz}, and σ_{yz} are the tractions required on the crack faces to close the crack over the distance Δa. The coordinate system is shown in figure 2.

The various approximations made in plate theory make equation (1) not directly applicable for calculating G. For example, plate theory does not provide the magnitude of the terms in equation (1). However, the concept of crack closure is still valid for plate analysis. The problem is to determine what is meant by closing a crack in plate analysis. In the following explanation of the new crack closure technique, Kirchhoff-Love plate theory is assumed.

Figure 3 shows the crack-front region of a plate with a single delamination. As shown in the figure, the intact plate (region A) is split at the crack-front into two sublaminates. Although the plate regions are shown with some thickness, the only gradient through the thickness is the linear variation of u and v due to the rotations $-w_{,x}$ and $-w_{,y}$. Because of this simplified response in the thickness direction, there is an abrupt change in the response of the plate from the uncracked region to the cracked region. For example, the curvature k_x of region A at the crack front is different from k_x of region B at the crack-front. Closure of the crack-front over an infinitesimal distance Δa implies the following:

> Over the distance Δa, the two sublaminates (regions B and C) behave as a single intact plate after closure. That is, u, v, ε_x, ε_y, and ε_{xy} vary linearly and w is constant through the entire thickness of the combined plate (B + C) over the distance Δa. Since Δa is infinitesimal, the strain distribution through the thickness of the sublaminates after closure is the same as in the intact plate at the crack front.

Work is required to impose the closure, since midplane strains and curvatures must be changed. This required work per unit area of crack closure is equal to the strain-energy release rate.

The first step in the derivation of a mathematical formula for strain-energy release rate is to express the strain distributions in regions A, B, and C. These are given in equations (2).

$$\varepsilon_i^A = \varepsilon_{iO}^A + k_i^A z$$

$$\varepsilon_i^B = \varepsilon_{iO}^B + k_i^B (z - z_B) \qquad i = 1,3 \qquad (2)$$

$$\varepsilon_i^C = \varepsilon_{iO}^C + k_i^C (z - z_C)$$

where

$$\varepsilon_1 = \varepsilon_x;\ \varepsilon_2 = \varepsilon_y;\ \varepsilon_3 = \varepsilon_{xy}$$

$$k_1 = k_x;\ k_2 = k_y;\ k_3 = k_{xy}$$

z_B, z_C = z-coordinates of midplane of sublaminates B and C, respectively and ε_{iO}^A, ε_{iO}^B, and ε_{iO}^C are the midplane strains

To make the strain distributions through the thickness of regions B and C the same as for region A requires the following strain increments:

For region B,

$$\Delta\varepsilon_i^B = \varepsilon_i^A - \varepsilon_i^B = \left(\varepsilon_{iO}^A - \varepsilon_{iO}^B + k_i^A z_B\right) + \left(k_i^A - k_i^B\right)(z - z_B)$$

For region C, (3)

$$\Delta\varepsilon_i^C = \varepsilon_i^A - \varepsilon_i^C = \left(\varepsilon_{iO}^A - \varepsilon_{iO}^C + k_i^A z_C\right) + \left(k_i^A - k_i^C\right)(z - z_C)$$

where i = 1,3

Note that equations (3) express the strains in terms of each of the sublaminate coordinate systems. Equations (3) show that in general there is a change in both the midplane strain and the curvature. For each sublaminate equations (3) can be expressed as

$$\Delta\varepsilon_x = \Delta\varepsilon_{xO} + \Delta k_x z'$$

$$\Delta\varepsilon_y = \Delta\varepsilon_{yO} + \Delta k_y z' \qquad (4)$$

$$\Delta\varepsilon_{xy} = \Delta\varepsilon_{xyo} + \Delta k_{xy} z' = \Delta\varepsilon_{xyo}$$

where z' is either $z - z_B$ or $z - z_C$, depending on which region is being considered.

In equations (4) the twist curvature term Δk_{xy} is zero. This is a consequence of the slope compatibility requirement at the crack front, as explained next. Consider the crack front to be along a line x = constant. Along the crack front $\frac{\partial w}{\partial x}$ is continuous because of slope compatibility requirements. Since $\frac{\partial w}{\partial x}$ is continuous regardless of the value of y, the change in $\frac{\partial w}{\partial x}$ in the y-direction, $\frac{\partial}{\partial y}\frac{\partial w}{\partial x}$, must also be continuous. Since $k_{xy} = -2\frac{\partial^2 w}{\partial x \partial y}$, the twist k_{xy} must be continuous at the crack front and hence $\Delta k_{xy} = o$. Similar arguments can be made if the crack is along a line y = constant.

To impose the required mid-plane strain and curvature changes $\Delta\varepsilon_i$ and Δk_i requires in-plane stress and moment resultants for each sublaminate.

The magnitudes of the in-plane stress resultants and moments are determined using the sublaminate constitutive matrix, that is

$$\begin{bmatrix} \Delta N_x \\ \Delta N_y \\ \Delta N_{xy} \\ \Delta M_x \\ \Delta M_y \\ \Delta M_{xy} \end{bmatrix} = \begin{bmatrix} [A] & [B] \\ [B]^t & [D] \end{bmatrix} \begin{bmatrix} \Delta\varepsilon_{xO} \\ \Delta\varepsilon_{yO} \\ \Delta\varepsilon_{xyO} \\ \Delta k_x \\ \Delta k_y \\ \Delta k_{xy} = O \end{bmatrix} \tag{5}$$

The strain-energy release rate is simply the work required to change the mid-plane strains and curvatures in the cracked part of the plate at the crack front so that they are equal to the midplane strains and curvatures in the uncracked part of the plate at the crack front. This work is given by equation (7).

$$G = \frac{1}{2}\left(\Delta N_x^B \Delta\varepsilon_{xO}^B + \Delta N_y^B \Delta\varepsilon_{yO}^B + \Delta N_{xy}^B \Delta\varepsilon_{xyO}^B + \Delta M_x^B \Delta k_x^B + \Delta M_y^B \Delta k_y^B + \Delta M_{xy}^B \Delta k_{xy}^B + \text{similar terms for plate C}\right) \tag{6}$$

For a particular problem, many of the terms in equation (6) may be zero. If there is more than one delamination, the procedure is still the same, one simply has more sublaminates to consider. Equation (6) will be used later in this paper to calculate the distribution of G for several configurations.

Cases Analyzed

Two cases were examined: a transversely loaded square laminate and a post-buckled laminate in compression (fig. 4a). Figure 4b shows the plan view of the laminate and the delaminated region. The deformed profile is shown in figure 4c.

The transversely loaded laminate was used to illustrate and evaluate the VCCT. It was selected because an exact solution is available for the displacements and boundary stress resultants [ref. 10]. This case consists of two isotropic plates bonded together except for a square region. The lower and upper plates will be referred to as the base laminate and the sublaminate, respectively. The base laminate is assumed to be rigid. The sublaminate has a Young's modulus of 207 GPa and a Poisson's ratio of 0.3. The loading consists of a single transverse point load applied at the center of the sublaminate. The displacements are assumed to be small, so that linear analysis is adequate.

The second case was selected to represent a compressively loaded laminate with an embedded delamination (see fig. 4a). The configuration is very similar to the transversely loaded laminate. The loading is in-plane (instead of transverse) and, although the lower plate is much stiffer than the top plate, it is not rigid. The sublaminate is isotropic with a Young's modulus of 53.3 GPa and a Poisson's ratio of 0.31. The thickness of the sublaminate is 0.51 mm. Again, the lower and top plates will be referred to as the base laminate and sublaminate, respectively.

The deformation in the base laminate is assumed to be unaffected by the response of the sublaminate. Hence, the base laminate is in a state of uniaxial stress. The displacements of the base laminate are given by

$$u = x\varepsilon_x$$

$$v = -y\nu_{xy}\varepsilon_x$$

The slope at the sublaminate boundary is zero.

Closed Form Analyses

Two closed form stress analyses were used to analyse the transversely loaded square plate: a Rayleigh-Ritz (R-R) analysis [ref. 10] and an exact series solution [ref. 11]. The R-R analysis was used to evaluate the performance of the VCCT when an approximate stress analysis is used to obtain the terms in equation (7). The exact solution provided a reference for evaluating the accuracy of the VCCT when the terms in equation (7) are known exactly. The key equations from the R-R analysis in reference 10 are:

$$w(x,y) = \sum_{m=1}^{3}\sum_{n=1}^{3} a_{mn}\left[1 - (-1)^m \cos\left(\frac{2m\pi x}{a}\right) - (-1)^n \cos\left(\frac{2n\pi y}{a}\right)\right] \qquad (7)$$

where

$$a_{11} = 0.12662\ \bar{P} \qquad a_{12} = a_{21} = -0.00601\ \bar{P}$$

$$a_{22} = 0.00301\ \bar{P} \qquad a_{13} = a_{31} = 0.00278\ \bar{P}$$

$$a_{33} = 0.0015\ \bar{P}$$

and the normalized load $\bar{P} = \dfrac{Pa^2}{\pi^4 D_{11}}$. The maximum displacement w_o under the load P is

$$w_o = .005435\ Pa^2/D_{11} \tag{8}$$

The key equations from the exact solution in reference 11 are

$$w_o = .0056\ \frac{Pa^2}{D_{11}} \tag{9}$$

and an expression for the curvature k_x along $x = a/2$

$$k_x = \frac{1}{D_{11}} \sum_{m=1,3,5,7,\ldots} (-1)^{\frac{m-1}{2}}\ Q_m \cos \frac{m\pi y}{a} \tag{10}$$

where $Q_1 = -0.1025\ P$

$Q_3 = 0.0263\ P$

$Q_5 = 0.0042\ P$

$Q_7 = 0.0015\ P$

Only the first four terms were retained, since addition of the fifth term changed k_x by only 0.32 percent. Because of symmetry, the distribution of k_y along $y = a/2$ is identical to that of k_x along $x = a/2$.

Finite Element Analysis

The STAGSC-1 [ref. 12] finite element program was used to analyse the configurations considered. Linear analysis was used for the transversely loaded laminate and geometrically nonlinear analysis was used for the postbuckled sublaminate. The following subsections describe the finite element models and how the VCCT is used with finite elements.

Finite element models.- Figures 5 and 6 show typical finite element models used for the transversely loaded laminate and the postbuckled sublaminate, respectively. Boundary conditions are indicated in the figures. Because of symmetries about the x- and y-axis, only one fourth of the subplate is modeled for both configurations. The elements are non-conforming, four-node quadrilaterals with six degrees of freedom (three displacements and three rotations) at each node. The STAGSC-1 program refers to this element as type 410. The penalty function option was selected to reduce incompatibilities in the displacements at the element boundaries.

The results presented herein were obtained with meshes graded in the x- and y-directions. This was found to give better results than a uniform mesh with the same number of elements. The grading of the mesh resulted in a fine mesh at one corner (eg. the upper right hand corner of the mesh in fig. 5). This fine mesh at the corner is just an artifact of the grading, not any intention to model the corner more accurately than elsewhere. Several different mesh refinements were examined to assure that the trends were correct.

Virtual crack closure technique for finite elements.- Theoretically, use of VCCT with finite elements is straight forward. Simply use the mid-plane strains and curvatures in regions A, B, and C (see fig. 3) at the crack front in equations (3), (4), (6), and (7). Unfortunately, many finite elements programs (including STAGSC-1) do not output the required quantities right at the crack front. For example, results may be provided at the quadrature points. In this case, one might extrapolate to the crack front. In general, some engineering judgement will be required to use the information provided by a finite element program to estimate the information required to calculate G.

In this study, reactions at the boundary of the finite element model were used to calculate the required information. This was possible because only the sublaminate was modeled; hence, the crack front was at the model boundary. The procedure used to extract the required information from the nodal reactions is described next.

The boundary nodal reactions are the equivalent forces and concentrated moments which are required to impose the specified boundary conditions. For example the postbuckled sublaminate has specified nonzero in-plane displacements and zero slope along the edges $x = \pm a/2$ and $y = \pm b/2$. To impose these conditions requires a distribution of mid-plane stresses and moments along these edges. The concentrated nodal moments and forces are statically equivalent to these distributed stresses and moments. A step variation of the moments was assumed along the edge (see fig. 7). The concentrated moment at a node was assumed to be equal to the integral of the distributed moment from the middle of the element on the left of the node to the middle of the element on the right. Nodes at the corners of the models had contributions from only one side. This simple assumption means that the distributed moment is equal to the concentrated moment divided by the length. The mid-plane stress resultants were calculated using this same procedure.

RESULTS AND DISCUSSION

First, details of the application and accuracy of the VCCT will be discussed for the transversely loaded laminate. The transversely loaded laminate is used because there is an exact, closed form solution for the plate deformations. Hence, the exact value of the average G along the delamination front can be calculated and used as a reference. Of course, it would be preferable to have a reference solution for the distribution of G, but one is not available.

Next, the effect of several parameters on G for postbuckled delaminations will be discussed.

Application of the VCCT

Because of symmetry only one-eight of the perimeter of the transversely loaded plate need to be considered when applying the VCCT. In particular, the crack front along $x = a/2$ for $0 \leq y \leq a/2$ will be analyzed. The plate deflections are assumed to be small. Hence, the mid-plane strains are zero throughout; therefore, $\Delta\varepsilon_{xO} = \Delta\varepsilon_{yO} = \Delta\varepsilon_{xyO} = 0$. Along $x = a/2$, the curvature k_y is zero for both the intact and the debonded region at the crack tip; therefore, $\Delta k_y = 0$. The curvature k_x is zero throughout the lower plate, since it is assumed to be rigid. The top plate has zero k_x in the bonded region and a non-zero k_x in the debonded region. Therefore, the strain-energy release rate, using equation (7), is

$$G = \frac{1}{2} (\Delta k_x \, M_x) \tag{11}$$

where $\Delta k_x = -$ (k_x of the unbonded top plate at the crack tip)

$$k_x = \frac{\partial^2 w}{\partial x^2}$$

and

$$M_x = D_{11} \, \Delta k_x$$

Figure 8 shows the distribution of normalized G along $x = a/2$ obtained using several analyses. In all cases the VCCT was used to calculate G. The R-R solution used equation (7) to determine k_x. The exact solution used equation (10) to determine k_x. All three analyses predict a strong gradient of G along $x = a/2$. Growth of the delamination should occur preferentially in the middle of the sides, thus transforming the square into a rounded shape. The finite element results agree well with the exact solution. The R-R analysis predicts the same trend as the exact solution but the magnitudes are different. The large differences between the R-R and exact analyses are due to the errors in calculating boundary curvature and moment with the R-R analysis.

Average values of G for the crack front were calculated using the VCCT and by differentiating the strain energy with respect to "a". Although not a complete check, comparison of the results should give some indication of the accuracy of the VCCT. The average G was calculated using the VCCT by integrating the results in figure 8 and dividing by the length of the crack front (eq. (12)).

$$G_{av} = \frac{2}{a} \int_{o}^{a/2} G \, dy \tag{12}$$

The strain-energy derivative technique (SEDT) uses the following expression for average G.

$$G_{av} = \frac{P}{4a} \frac{\partial w_o}{\partial (a/2)} - \frac{1}{4a} \frac{\partial U}{\partial (a/2)} \tag{13}$$

The derivative is taken with respect to a/2 because the delamination is assumed to extend in a self-similar manner. For example, the boundaries at $x = \pm a/2$ moves to $x = \pm (a/2 + \Delta(a/2))$.

The strain energy U can be expressed as

$$U = \frac{1}{2} P w_o \tag{14}$$

From equations (13) and (14) we obtain

$$G_{av} = \frac{P}{4a} \frac{\partial w_o}{\partial a} \tag{15}$$

The average G obtained using the VCCT and the strain-energy derivative technique (eq. (13)) are

	$G_{av}D_{11}/P^2$
Exact	0.002804 (VCCT)
	0.002800 (SEDT)
Finite Elements	0.002744 (VCCT)
R-R	0.002229 (VCCT)
	0.002717 (SEDT)

There is essentially no difference between the average G obtained with the VCCT and equation (15) when the exact solution is used. (The small difference is a result of using only the first four terms in the series solution.) The VCCT itself is apparently accurate, but the accuracy of the calculated G depends on the stress analysis used. When calculating average G with an approximate analysis, (i.e. the R-R analysis) the VCCT is considerably less accurate than the strain energy derivative technique.

Generally one would want to know the distribution of G rather than just an average value. If an approximate analysis is being used, equation (15) gives a better estimate of average G than using equations (11) and (12). A reasonable compromise is to use equation (15) to obtain the average G and use equation (11) to obtain the distribution of G. Then scale the G distribution such that the VCCT gives the same average G. The curve labeled "scaled R-R" in figure 8 was obtained by using this procedure. The agreement with the exact solution is good.

Postbuckled Sublaminate

The VCCT described in the previous sections was used to calculate G for the compressively loaded specimen shown in figure 4. The effect of delamination dimensions and strain level on the magnitude and distribution of G is illustrated in figures 9-12.

For the postbuckled sublaminate, the equation for calculating G (eq. (6)) reduces to

$$\underline{\text{along } x = a/2}$$

$$G = 1/2 \left(\Delta N_x^B \, \Delta\varepsilon_{xO}^B + \Delta M_x^B \, \Delta k_x^B \right) \tag{16}$$

$$\underline{\text{along } y = b/2}$$

$$G = 1/2 \left(\Delta N_y^B \, \Delta\varepsilon_{yO}^B + \Delta M_y^B \, \Delta k_y^B \right)$$

where

$$\Delta\varepsilon_{xO}^B = \varepsilon_x - e_O$$

$$\Delta\varepsilon_{yO}^B = \varepsilon_y + \nu e_O$$

$$\Delta k_x^B = k_x$$

$$\Delta k_y^B = k_y$$

e_O = strain in x-direction in base laminate

Equation (21) shows that G consists of contributions from changes in both mid-plane strain and curvature. The contributions from changes in the mid-plane strain and curvature are referred to herein as G_N and G_M, respectively.

Figure 9 shows the distribution of G_N and G_M for 25.4 × 25.4 mm and 25.4 × 50.8 mm delaminations (solid and dashed curves, respectively). The first dimension refers to the length in the x-direction. The applied strains for the 25.4 × 25.4 mm and 25.4 × 50.8 mm delaminations were -0.0040 and -0.0043 respectively. The bifurcation buckling strains were -0.0037 and -0.0018, respectively.

For the square delamination (solid curves), the magnitudes of G_N and G_M are much larger along $y = b/2$ (fig. 9b) than along $x = a/2$ (fig. 9a). Hence, one would expect an initially square delamination to grow transverse to the load direction (in the y-direction). Since G_M and G_N are much smaller near the corners of the delamination, the delamination would not grow in a self-similar fashion. Instead, it would become more like an ellipse than a rectangle. Note that G_M is much larger than G_N for the delamination front along both $x = a/2$ and $y = b/2$. For the rectangular (25.4 × 50.8) delamination the maximum value of the sum of G_M and G_N is about 300 J/m^2 for both $x = a/2$ and $y = b/2$. Hence, one might expect the delamination to grow equally in the x- and y-directions, initially maintaining an aspect ratio (b/a) of about 2 and becoming elliptical. However, the aspect ratio for equal growth in the x- and y-directions depends on the absolute size of the delamination and the strain level. This is discussed next.

Figure 10 shows G ($G = G_M + G_N$) for the 25.4 × 50.8 mm and 50.8 × 101.6 mm delaminations with an applied strain of -0.0034. Along $y = b/2$ (fig. 10b), the larger delamination has a G which is more than twice as large as G along $x = a/2$ (fig. 10a). Hence, growth should occur more rapidly along $y = b/2$, resulting in an aspect ratio of more than 2. The smaller delamination in figure 10 was also subjected to a strain of -0.0034. Note that figure 10 predicts the smaller delamination will grow in the loading direction (because of the larger G), which will reduce the aspect ratio to less than 2.

The peak values of G from figures 9 and 10 are combined in figure 11. The square delamination is clearly expected to grow more easily transverse to the load direction. The behavior of the 25.4 × 50.8 mm delamination depends on the strain level. At the lower strain level, growth is expected to occur preferentially in the load direction, but at the higher strain level, the growth rates are expected to be about the same in both directions. Although the 50.8 × 101.6 mm delamination has the same aspect ratio as the smaller rectangular delamination, figure 11 shows that the larger rectangular delamination will grow preferentially transverse to the load direction. Note that e_o/e_{CR} is 7.6 for the larger delamination, which is much larger than for the load cases for the smaller delamination. Apparently, as the strain becomes larger relative to the buckling strain, there is a greater tendency for the delamination to grow transverse to the load direction instead of along the load direction.

Figures 9 and 10 suggest that at least for some configurations, delamination growth would be unstable if it is governed by G. In each case, the peak G is larger for the larger delamination when the applied strain is constant (approximately). Of course, a rectangular delamination does not grow to be a larger rectangular delamination; it becomes elliptical. But the large difference in G between the smaller and larger delaminations in figures 9 and 10 probably outweighs the

differences due to modeling as a rectangle instead of as an ellipse. More configurations need to be analyzed to determine whether the delamination arrests when it grows very large.

The relative magnitudes of G_N and G_M depend both on the size of the delamination and the edge examined. Figure 9 shows that for the 25.4 × 50.8 delamination G_N is a significant protion of G along $x = a/2$, but it is insignificant along $y = b/2$. For the 25.4 × 25.4 mm delamination G_N is insignificant along $y = b/2$. For the 25.4 × 25.4 mm delamination G_N is insignificant along both edges for a strain of -0.004.

Figure 12a shows the effect of strain level on the magnitudes of G_N and G_M along $x = a/2$ for the 25.4 × 25.4 delamination. Dashed and solid lines are used for G_M and G_N, respectively. The peak value of G_N decreased as the strain increased. Conversely, G_M increased monotonically. One of the G_N curves is marked "switched mode". For this strain level, the plate has changed from the first buckling mode to a higher mode. This can result in negative displacements, which are physically impossible since the base laminate will not allow this. Further work (beyond the scope of this paper) is needed to determine an accurate and efficient method for analyzing such cases. Figure 12b shows the effect of strain level on G_M along $y = b/2$. The magnitude of G_N is not shown because it was quite small for all cases. The magnitude of G_M increases rapidly as the strain increases.

CONCLUSIONS

A virtual crack closure technique was developed for calculating the distribution of total strain-energy release rate around the boundary of a delamination in a plate. This is an improvement over earlier techniques, which only provide an average of the strain-energy release rate along the delamination front. This technique was verified by analyzing a configuration with a closed-form exact solution for the average strain-energy release rate. The technique was then used to calculate the distribution of strain-energy release rate for several cases involving the postbuckling of a delaminated region. The following conclusions were reached.

1. The virtual crack closure technique developed herein appears to be an accurate technique for calculating the distribution of total strain-energy release rate.

2. For square and rectangular delaminations, there is a large variation of strain-energy release rate along the delamination front. Hence, self-similar growth is not expected.

3. Whether a delamination grows in the load direction or perpendicular to the load direction in a compressively loaded laminate depends on the current delamination aspect ratio, the strain level, and the absolute size of the delamination.

REFERENCES

1. Byers, B. A.: Behavior of Damaged Graphite/Epoxy Laminates Under Compression Loading. NASA CR-159293, August 1980.

2. Porter, T. R.: Compression and Compression Fatigue Testing of Composite Laminates. NASA CR-168023, July 1982.

3. Konishi, D. Y. and Johnson, W. R.: Fatigue Effects on Delaminations and Strength Degradation in Graphite/Epoxy Laminates. Composite Materials: Testing and Design, Fifth Conference, ASTM STP, American Society for Testing and Materials, 1979, pp. 597-619.

4. Whitcomb, J. D.: Strain-Energy Release Rate Analysis of Cyclic Delamination Growth in Compressively Loaded Laminates. Effects of Defects in Composite Materials, ASTM STP 836, American Society for Testing and Materials, Philadelphia, Pa., 1984, pp. 175-193.

5. Whitcomb, J. D.: Finite Element Analysis of Instability-Related Delamination Growth, J. Composite Materials. 15, 1981, pp. 403-426.

6. Whitcomb, J. D.: Parametric Analytical Study of Instability-related Delamination Growth. Composites Science and Technology, 25, 1986, pp. 19-48.

7. Chai, Herzl; Babcock, Charles D. and Knauss, Wolfgang G.: One Dimensional Modeling of Failure in Laminated Plates by Delamination Buckling. Int. J. of Solids Structures, Vol. 17, No. 11, 1981, pp. 1069-1083.

8. Chai, Herzl; Babcock, Charles D.: Two-Dimensional Modeling of Compressive Failure in Delaminated Laminates. Journal of Composite Materials, Vol. 19, January 1985, pp. 67-98.

9. Irwin, G. R.: Analysis of Stresses and Strains Near the End of a Crack Traversing a Plate. Journal of Applied Mechanics, Transactions of ASME, September 1957, pp. 361-364.

10. Ugural, A. C.: Stresses in Plates and Shells. McGraw-Hill, New York, 1981, p. 93.

11. Timoshenko, S. P. and Woinowski-Krieger, S.: Theory of Plates and Shells, McGraw-Hill, New York, 1959, pp. 203-206.

12. Almroth, B. O.; Brogan, F. A. and Stanley, G. M.: Structural Analysis of General Shells, Vol. 2, User Instructions for STAGSC-1. Lockheed Palo Alto Research Laboratory, Palo Alto, CA, 1982.

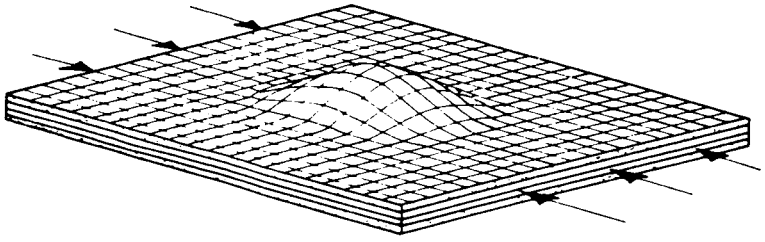

Figure 1.- Sketch of a locally postbuckled laminate with embedded delamination.

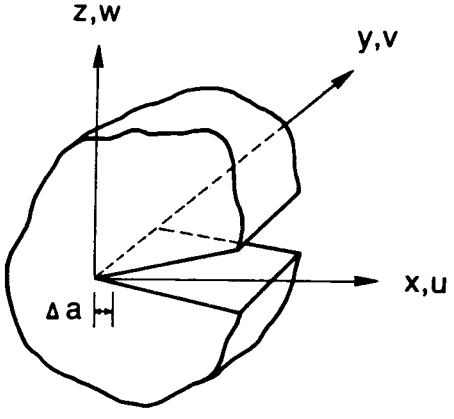

Figure 2.- Crack front region.

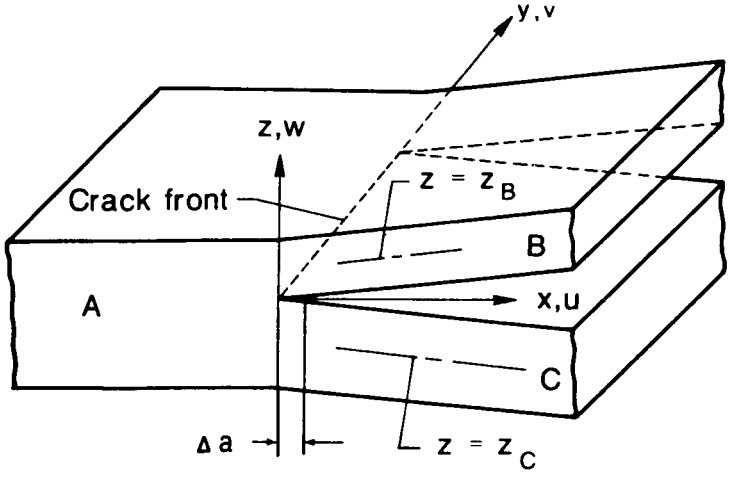

Figure 3.- Crack front region of a plate with single delamination.

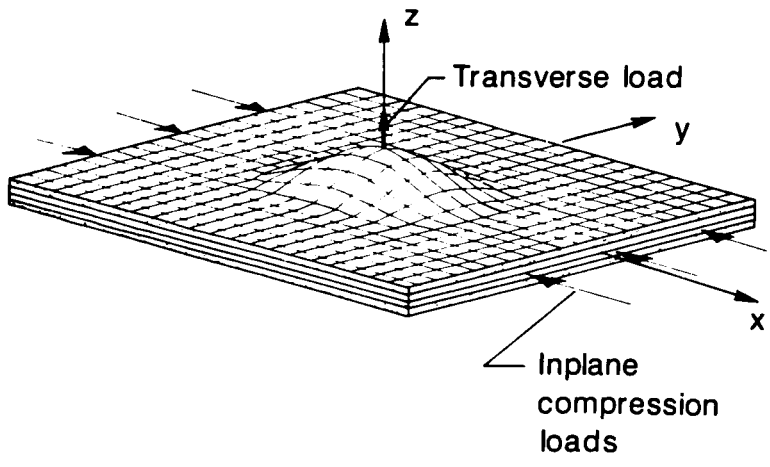

(a) Deformed laminate and two types of loading considered.

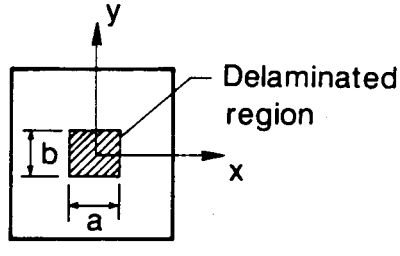

(b) Plan view of laminate.

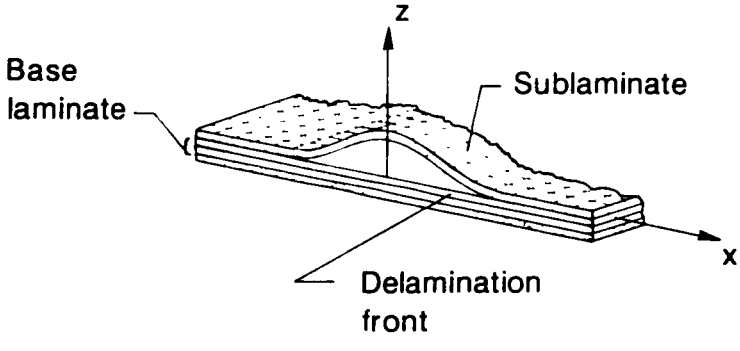

(c) Cross-section of deformed laminate.

Figure 4.- Laminate configuration and loading.

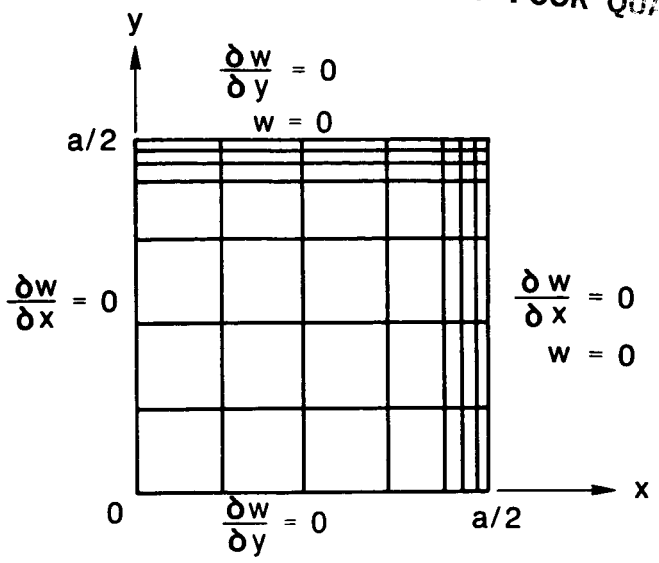

Figure 5.- Finite element model for transversely loaded sublaminate.

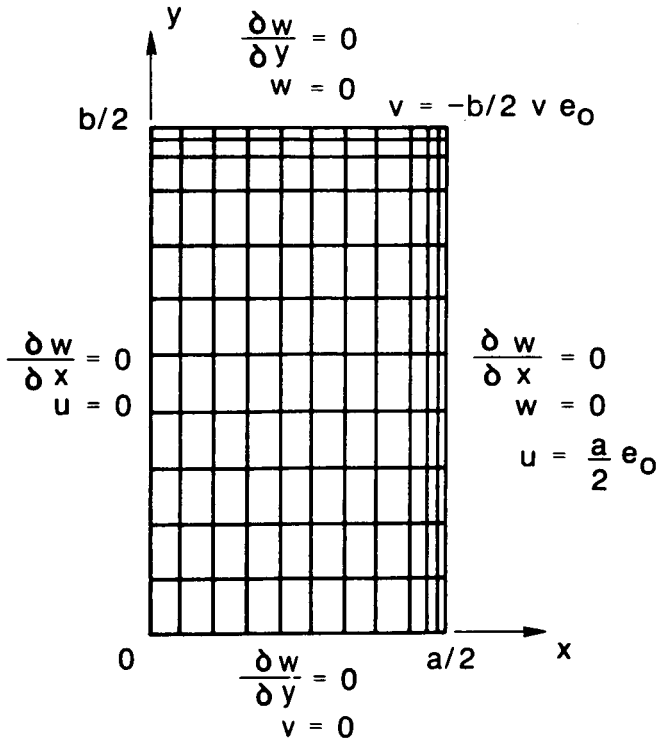

Figure 6.- Typical finite element model for a postbuckled sublaminate.

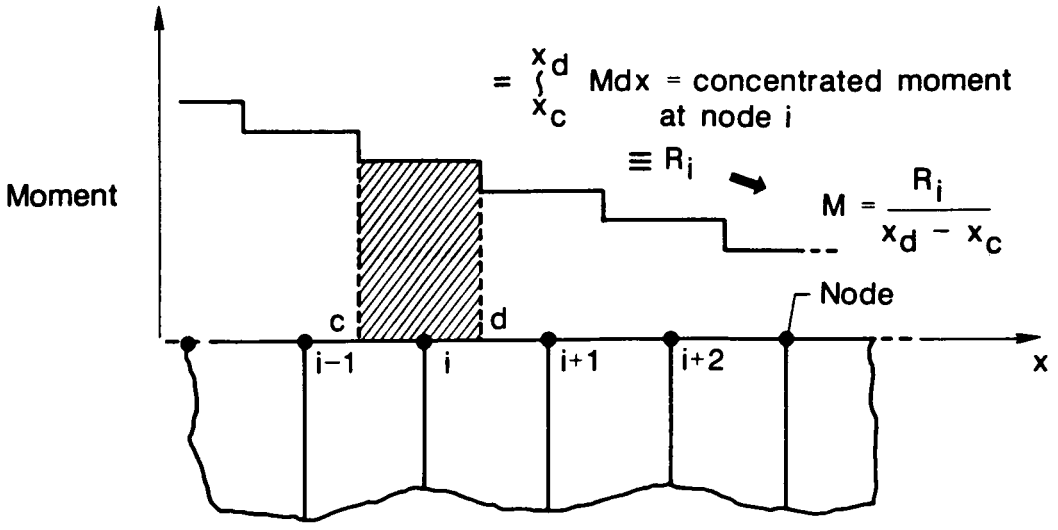

Figure 7.- Calculation of the moment distribution M from the nodal concentrated moment R_i.

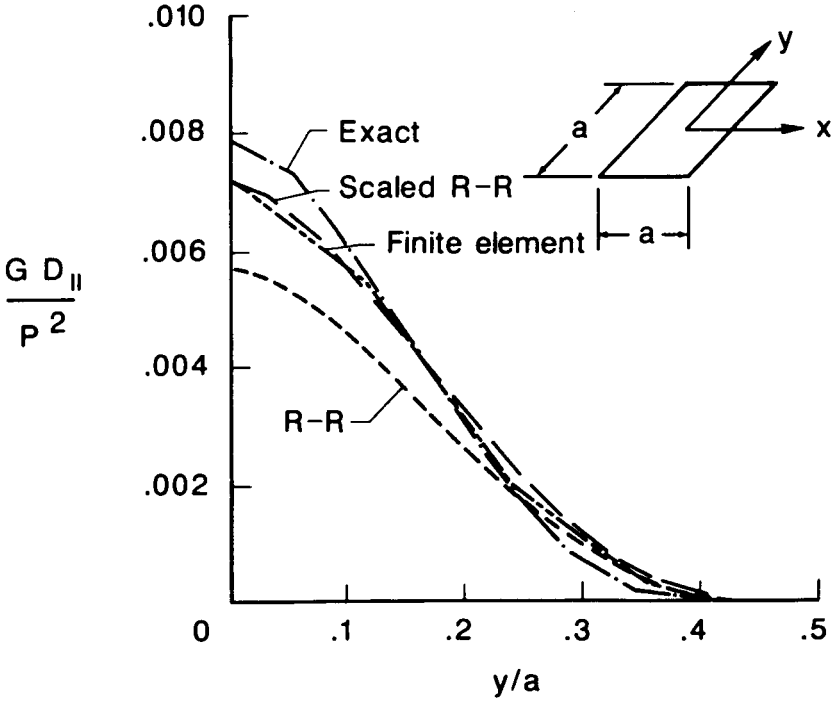

Figure 8.- Distribution of G along x = a/2 for transversely loaded sublaminate (a = b = 25.4 mm).

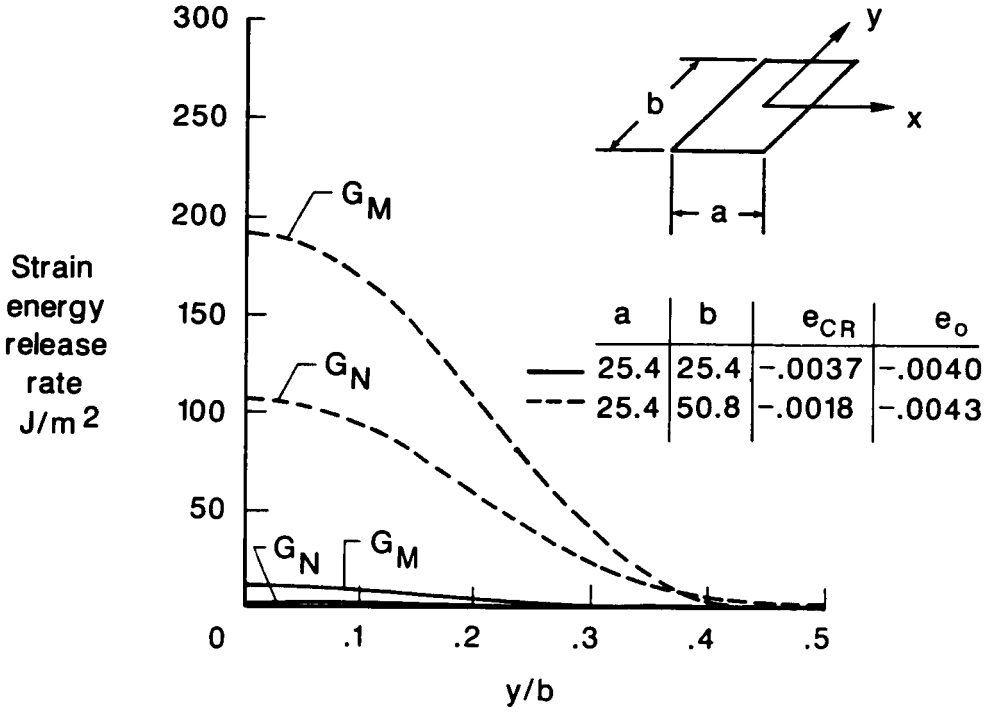

(a) Distribution along x = a/2

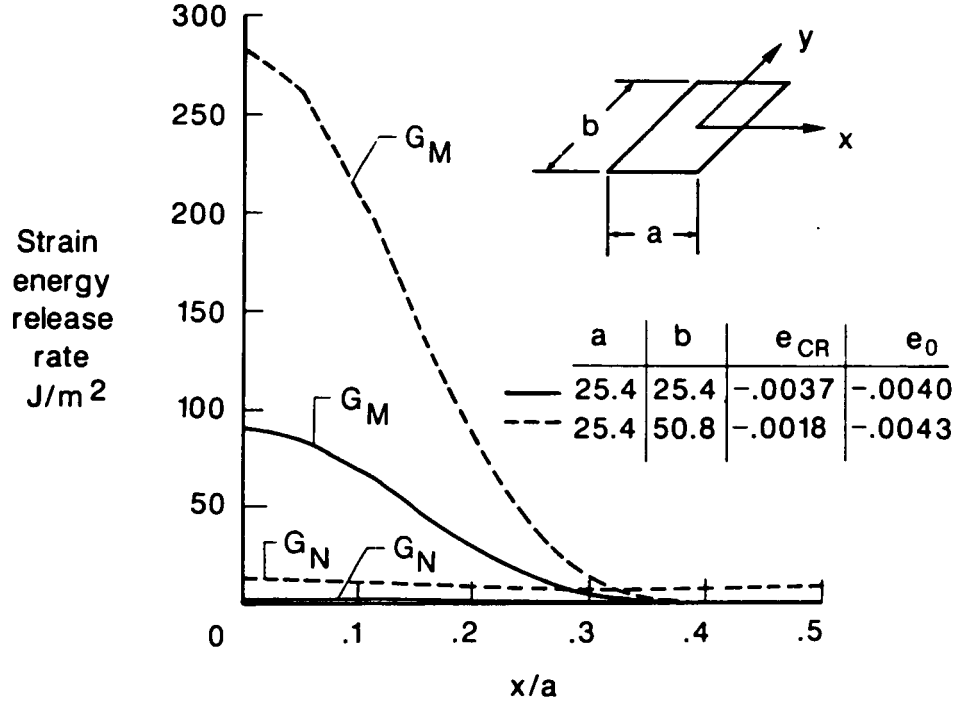

(b) Distribution along y = b/2

Figure 9.- Distribution of G_M and G_N for two postbuckled sublaminate along x = a/2 and y = b/2.

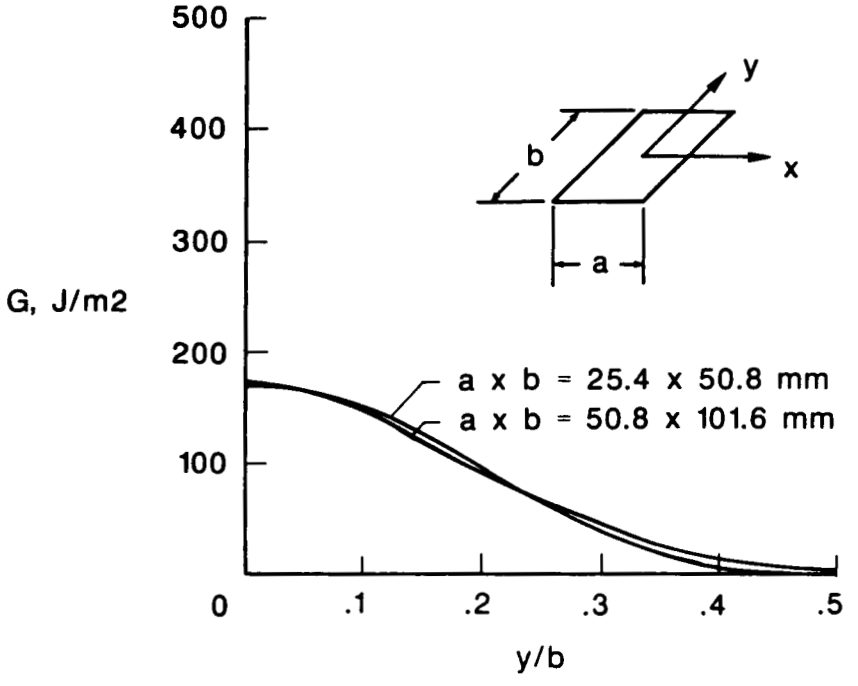

(a) Distribution along x = a/2

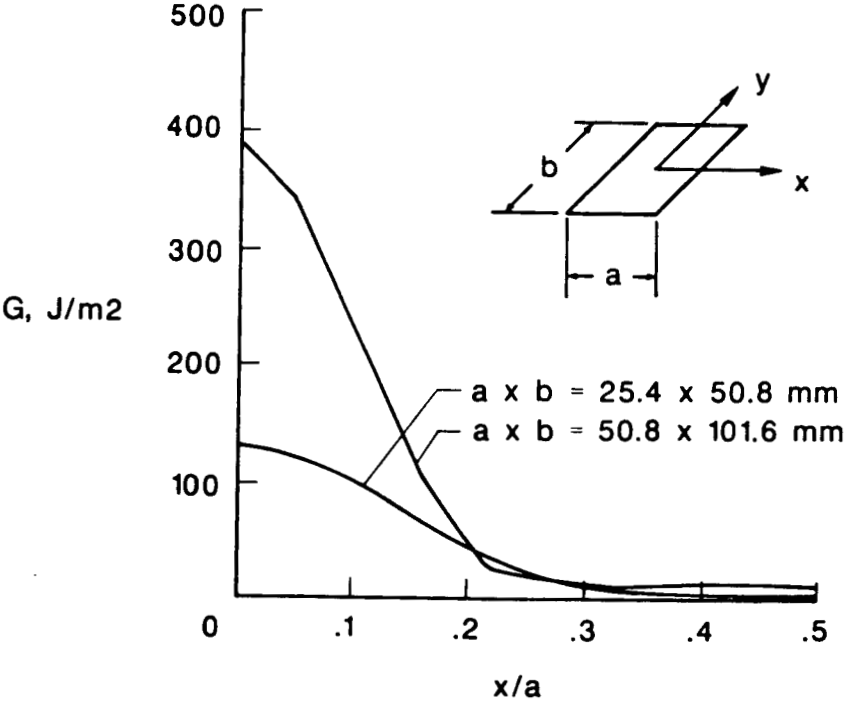

(b) Distribution along y = b/2

Figure 10.- Distribution of G for two different size delaminations with same aspect ratio (e = 0.0034).

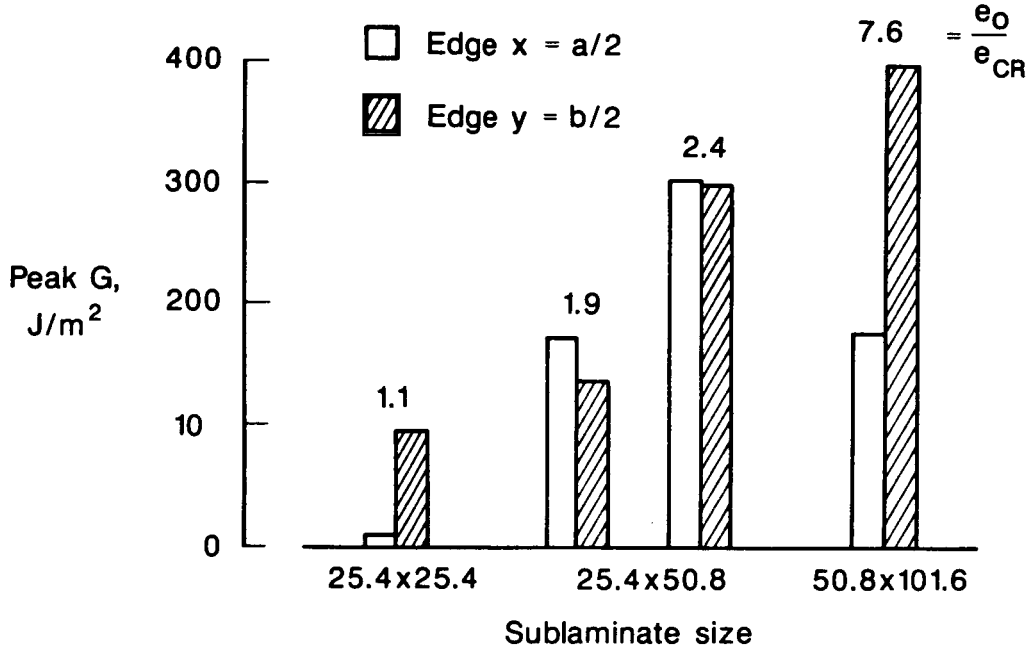

Figure 11.- Peak values of G for several sublaminate and loading cases.

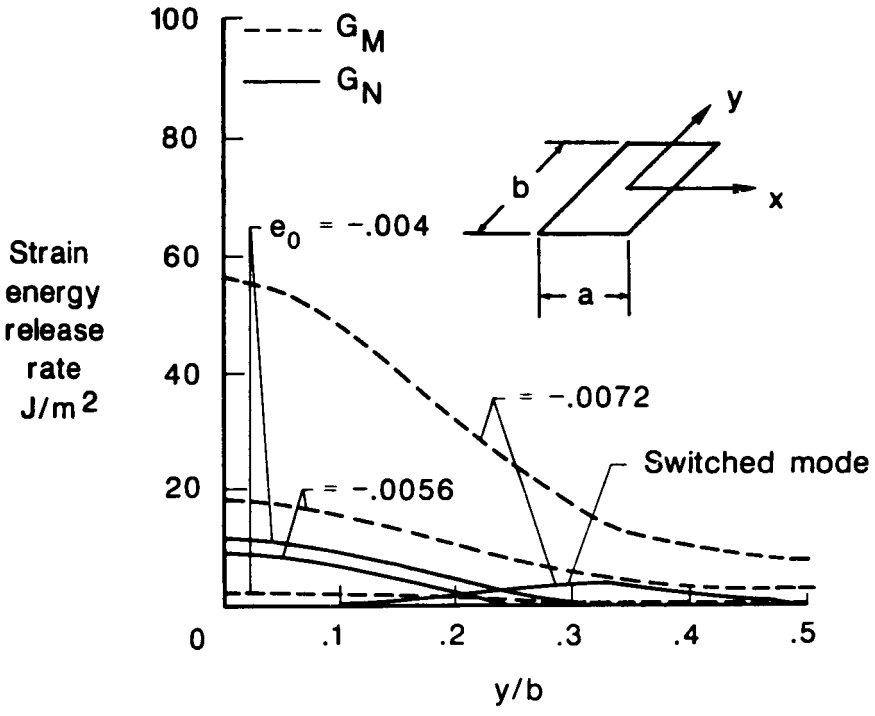

(a) Distribution along x = a/2

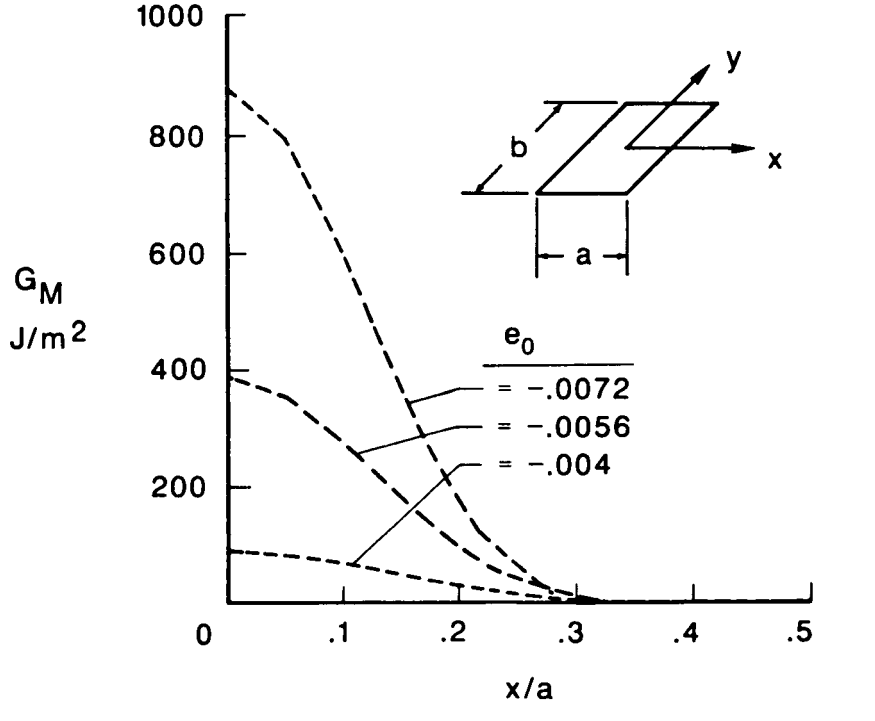

(b) Distribution along y = b/2

Figure 12.- Effect of strain level on G_M and G_N for a = b = 25.4 mm (G_N is not shown in fig. 12(b), because it is very small for all curves).

Standard Bibliographic Page

1. Report No.	2. Government Accession No.	3. Recipient's Catalog No.
NASA TM-89091		

4. Title and Subtitle	5. Report Date
Strain-Energy Release Rate Analysis of Plates with Postbuckled Delaminations	February 1987
	6. Performing Organization Code: 506-43-11-04
7. Author(s): John D. Whitcomb and K. N. Shivakumar*	8. Performing Organization Report No.
9. Performing Organization Name and Address: NASA Langley Research Center, Hampton, VA 23665-5225	10. Work Unit No.
	11. Contract or Grant No.
12. Sponsoring Agency Name and Address: National Aeronautics and Space Administration, Washington, DC 20546	13. Type of Report and Period Covered: Technical Memorandum
	14. Sponsoring Agency Code

15. Supplementary Notes

*K. N. Shivakumar, Analytical Services and Materials, Inc.,107 Research Drive, Hampton, VA 23666

16. Abstract

Delamination growth due to local buckling of a delamination was studied. Delamination growth was assumed to be related to the total strain-energy release rate, G. In order to calculate the distribution of G along the delamination front, a virtual crack closure technique was developed which is suitable for use with plate analysis. A check of the technique indicated that it is accurate. For square and rectangular delaminations, there is a large variation of G along the delamination front. Hence, self-similar growth is not expected. Whether a delamination grows in the load direction or perpendicular to the load direction was found to depend on the current delamination aspect ratio, the strain level, and the absolute size of the delamination.

17. Key Words (Suggested by Authors(s))	18. Distribution Statement
Buckling Local Buckling Compression Finite-element Delamination Strain-energy release rate	Unclassified - Unlimited Subject Category 24

19. Security Classif.(of this report)	20. Security Classif.(of this page)	21. No. of Pages	22. Price
Unclassified	Unclassified	23	A02

For sale by the National Technical Information Service, Springfield, Virginia 22161